Supplementary Figs

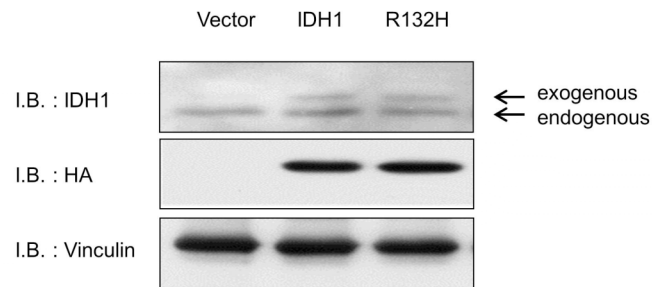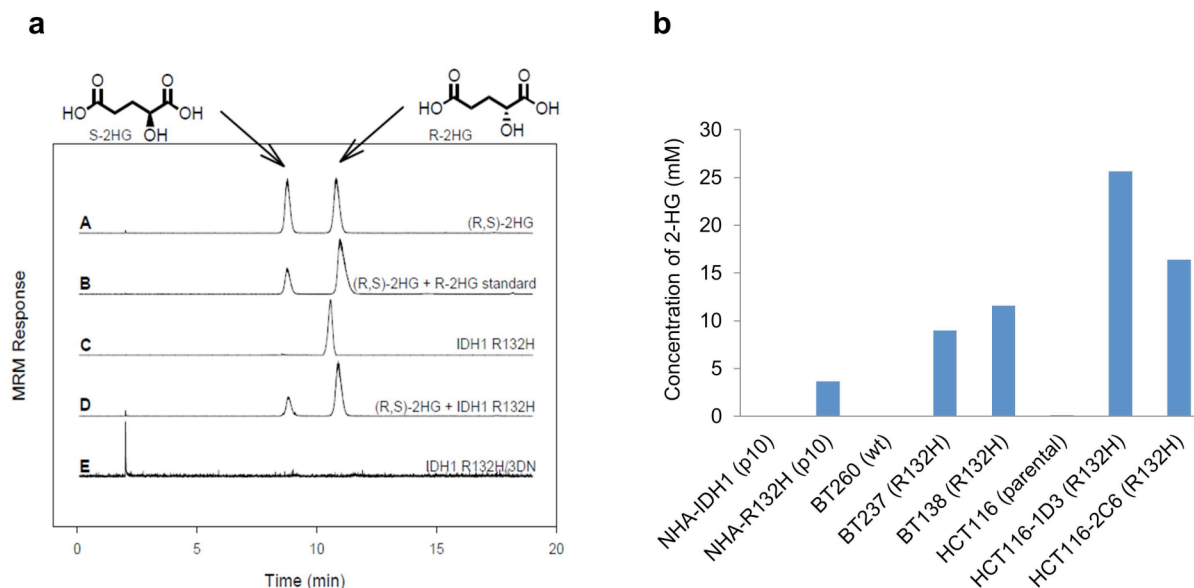|	Vector	IDH1	R132H	
I.B. : IDH1				← exogenous ← endogenous
I.B. : HA				
I.B. : Vinculin				

S1. Exogenous expression of IDH1

Anti-IDH1 (top panel) and anti-HA (middle panel) immunoblot analysis of immortalized human astrocytes (passage 23) with retroviruses encoding HA-tagged versions of the indicated IDH1 variants. Similar results were obtained at early passage.

S2. Cellular production of R-2HG in cells producing expressing IDH1 R132H

a, Production of R-2HG by immortalized human astrocytes (passage 6) producing expressing IDH1 R132H. Chirality of 2HG was determined as described previously[1]. A, racemic mixture of R- and S-2HG; B, racemate co-injected with R-2HG standard; C and E, cellular lysates from IDH1 R132H and IDH1 R132H/3D expressing cells, respectively. D, cellular lysate from IDH1 R132H cells coinjected with R-2HG standard. **b,** Estimated intracellular R-2HG concentrations of the indicated cell lines. Intracellular R-2HG was measured as described in [1].
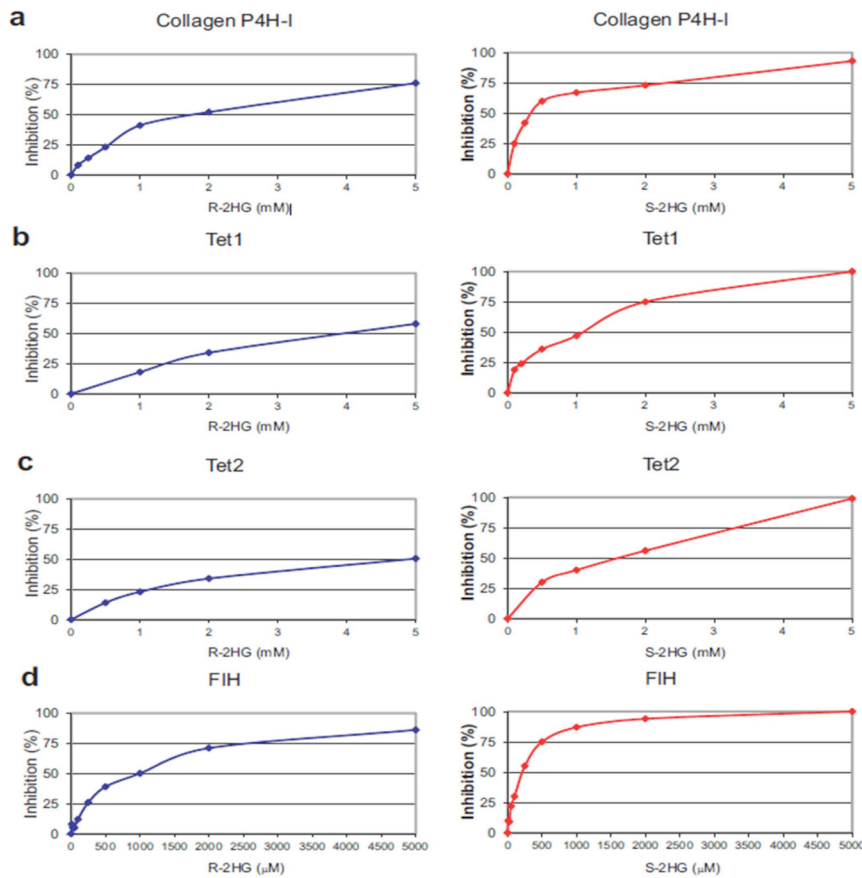
S3. Inhibition of 2-OG-dependent dioxygenases by 2HG.

**a-d,** Inhibition of collagen P4H-I (**a**), Tet1 (**b**), Tet2 (**c**) and FIH (**d**) by S-2HG and R-2HG.

Enzyme activities were determined with synthetic peptides (PPG)$_{10}$ (**a**) and

DESGLPQLTSYDCEVNAPIQGSRNLLQGEELLRAL (**d**) and a double stranded

oligonucleotide (5'-CTATACCTCCTCAACTT(mC)GATCACCGTCTCCGGCG-3'(**b,c**) as

substrates and decarboxylation of radiolabeled 2-OG was monitored. The 2-oxo-[1-^{14}C]glutarate

concentrations were 100 μM (**a**), 120 μM (**b,c**) and 10 μM (**d**).
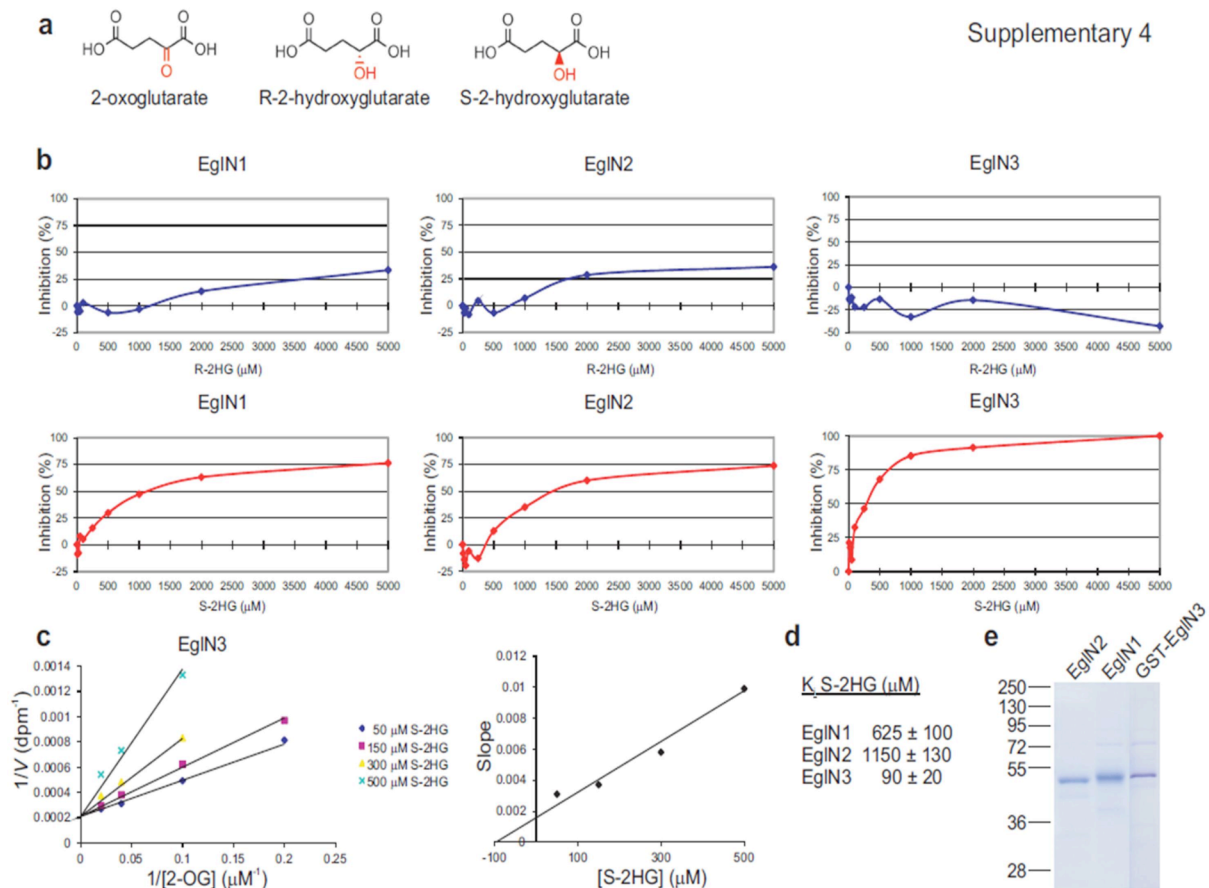
S4. S-2HG, but not R-2HG, inhibits EglN activity.

a, Structures of 2-oxoglutarate (2-OG), R-2-hydroxyglutarate (R-2HG) and S-2-hydroxyglutarate (S-2HG). **b,** Inhibition of EglN1-3 catalytic activity by increasing concentrations of R-2HG and S-2HG. Enzyme activity was determined with a synthetic 19-mer peptide (DLD19) spanning the HIF-1α P564 hydroxylation site as a substrate and monitored using decarboxylation of radiolabeled 2-OG. Concentration of the 2-oxo-[1-^{14}C]glutarate was 10 μM. **c** and **d,** S-2HG is a competitive inhibitor against 2-OG for EglNs. **e,** Coomassie Blue stained gel of EglNs used in these studies. The EglNs were affinity-purified from insect cells that had been infected with baculoviruses encoding either EglN2-Flag, EglN1-Flag, or GST-EglN3-Flag.
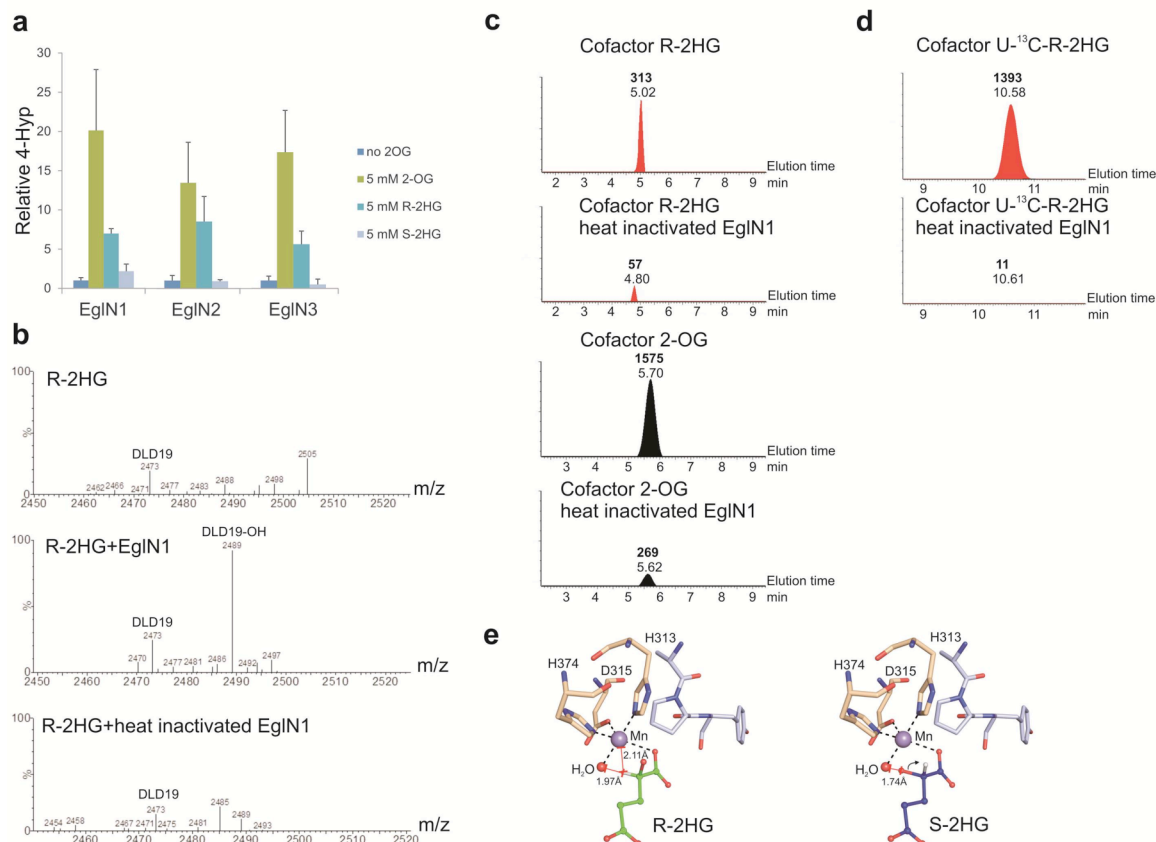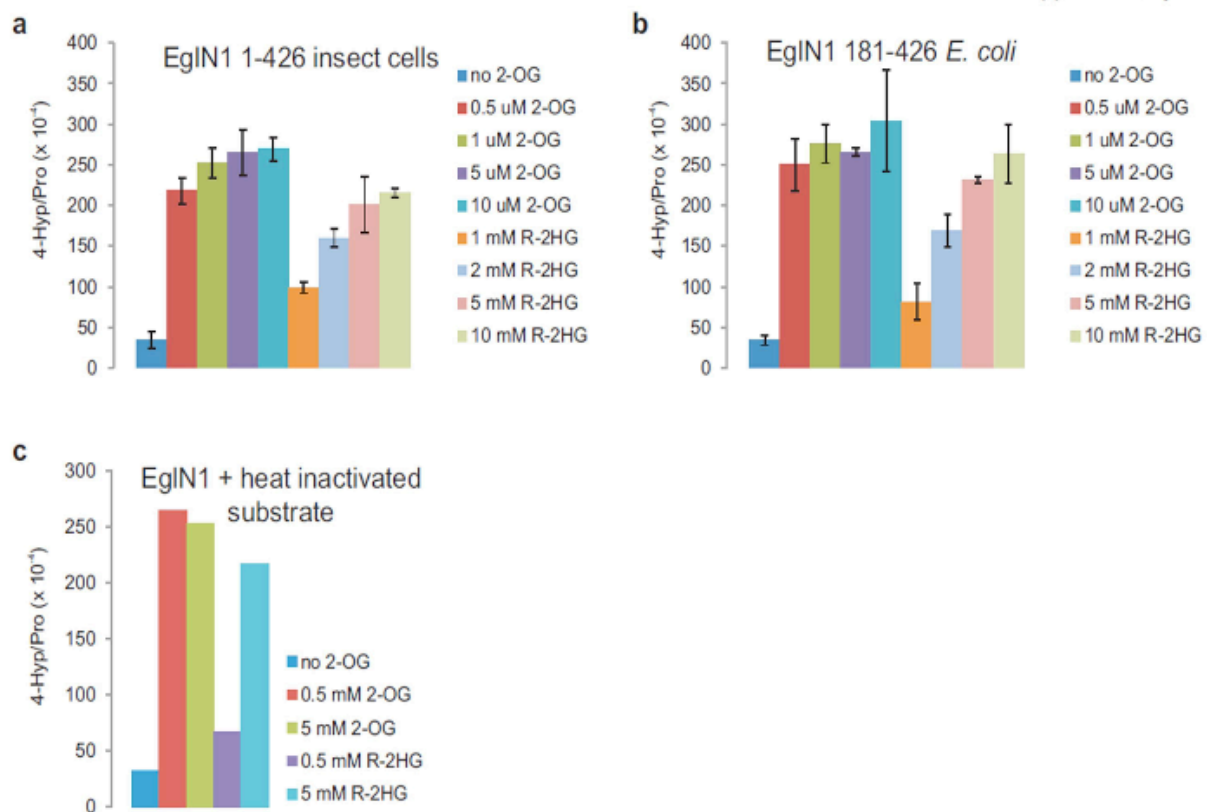
S5. Stimulation of EglN activity by R-2HG.

a, Shown is the amount of radioactive 4-Hyp generated by the three EglN family members in the presence of 5 mM 2-OG, R-2HG or S-2HG relative to the amount generated with no exogenous cofactor added (no 2-OG). In these assays, in contrast to Fig 2, the HIF1α oxygen-dependent degradation domain substrate was added at a concentration above the K_m for each enzyme (0.7 µM, 0.08 µM, and 0.36 µM for EglN1, EglN2, and EglN3, respectively) to insure that substrate was not limiting. The data are from replicates of 3 to 5 independent assays. **b,** HIF1α peptide in which Methionines were replaced by Alanines (DLDLEALAPYIPADDDFQL) was incubated at

37 °C for 20h in the presence of 5 mM R-2HG alone or with recombinant EglN1 purified from baculovirus-infected insect cells or EglN1 heat inactivated at 60 °C for 10 minutes prior to use. Methionines were eliminated to minimize spurious oxidation events. The HIF1α peptides were then analyzed by LC-MS/MS on a Synapt G2 ESI mass spectrometer (Waters). The HPLC column (Acquity UPLC BEH C18, 1.7µm, 2.1 × 50 mm, Waters) was operated at 20 °C at a flow of 0.5 ml/min with the gradient 0 min 2% B, 10 min 40% B, 12 min 95% B and 13 min 2% B. Solvent A: 0.1% formic acid and solvent B: acetonitrile+0.1% formic acid. Concentration of the HIF1α peptide in the sample was 50 µM and 10 µl aliquots of samples diluted in 1:5 were analyzed in triplicate. **c,** LC-MS analysis of succinate generated by EglN1 in the presence of a synthetic HIF1α peptide (DLD19) and either 5 mM R-2HG (red) or 100 µM 2-OG (black). Where indicated EglN1 was heat inactivated at 60 °C for 10 min prior to catalysis. Numbers next to each peak indicate elution times (plain font) and peak areas (bold font). The assay conditions differed from those in Fig. 2e in that the column was operated with 100 mM ammonium formiate pH 4 (98%) and acetonitrile (2%), which accounted for the delayed elution time of succinate compared to Fig. 2e. **d,** LC-MS analysis of ^{13}C-succinate generated by EglN1 in the presence of a synthetic HIF1α peptide (DLD19) and 5 mM uniformly labeled ^{13}C-R-2HG (Agios Pharmaceuticals) . Generation of ^{13}C-succinate was quantified by LC-MS in negative mode using multiple reaction monitoring (MRM) on a Quattro micro triple quadruple mass spectrometer (Waters). 40 µl aliquots of samples [4x the amount injected in (**c**)] were analyzed in triplicate. The HPLC column (Atlantis dC18, 5µm, 4.6 x150 mm, Waters) was operated at 30°C in speed of 0.5 ml/min in following buffer: 0 min 0.1% formic acid; 7.5 min 0.09% formic acid, 10% methanol; 12 min 0.087% formic acid, 13% methanol and 14 min 0.1% formic acid. The MRM transitions for ^{13}C-succinate were: 121>76, 121>103. **e,** Model of R-2HG (green) and

S-2HG (cyan) bound to the active site of EglN1 based on the crystal structure of EglN1 complexed with N-oxalylglycine and peptide substrate (PDB ID = 3HQR) showing the C2-hydrogen atoms of R-2HG and S-2HG in white. The peptide substrate is shown in light blue and the hydrogen bonds are indicated by black dash lines. Our data suggests a reaction mechanism in which R-2HG is first oxidized to 2-OG, which is then used as a cosubstrate in the prolyl 4-hydroxylation reaction. A step involving removal of the C2-hydrogen atom of R-2HG by an Fe(III)-superoxide intermediate must therefore occur. In case of R-2HG, the C2-hydrogen atom is directed towards Mn (purple) and H_2O (red), which represent the binding sites of Fe^{2+} and O_2, respectively, the distance of the C2-hydrogen atom to Mn being 2.11Å and that to H_2O 1.97Å, enabling removal of the C2-hydrogen atom by an Fe(III)-superoxide intermediate. In the case of S-2HG, the C2-hydrogen atom is directed away from the iron and oxygen binding sites the distances between the Fe^{2+} and O_2 binding sites and the C2-hydrogen atom being 2.79Å and 3.69Å, respectively. Importantly, the OH-group of S-2HG is located only 1.74Å from the oxygen binding site, which means that in order to bind to the hydroxylase the S-2HG molecule would have to rotate (shown by an arrow) to allow the OH-group to move away from the O_2 binding site, which would direct the C2-hydrogen atom even further away from the active site.

S6. Stimulation of EglN by R-2HG observed with different sources of enzymes and with heat-inactivated HIF1α polypeptide substrate

a-c, *In vitro* prolyl 4-hydroxylation assays conducted with recombinant 1 μM EglN1 produced in insect cells (EglN1 1-426) (**a,c**) or *E. coli* (EglN1 18-426) (**b**) in the presence of the indicated amounts of 2-OG or R-2HG and L-[2,3,4,5-³H]proline-labeled HIF1α oxygen-dependent degradation domain (ODDD) as the substrate. In (**c**) the HIF1α ODDD peptide was heated at 60 °C for 10 minutes prior to use. The *E. coli*-derived EglN1 was described before [2] and was a generous gift of Dr. Christopher Schofield.
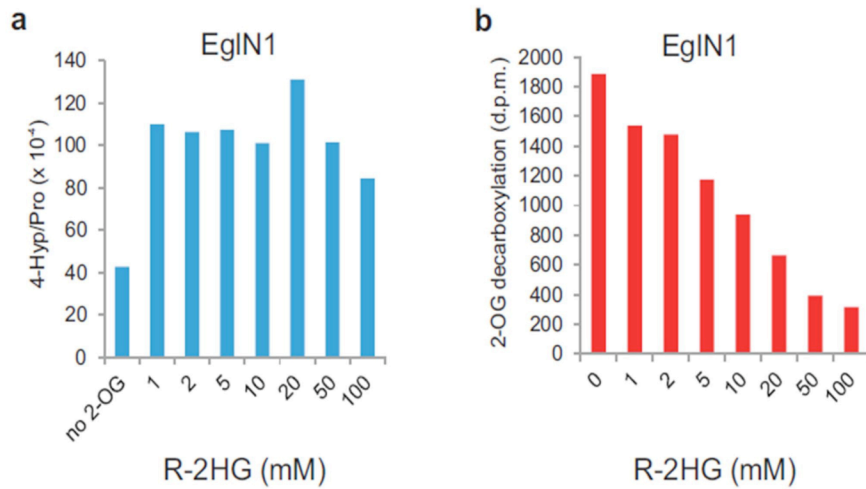
S7. Dissociation of HIF1α hydroxylation and 2-OG decarboxylation at high R-2HG concentrations

a,b, *In vitro* prolyl 4-hydroxylation assays conducted with recombinant EglN1 produced in insect cells and L-[2,3,4,5-^{3}H]proline-labeled HIF1α oxygen-dependent degradation domain (ODDD) produced in *E.coli* (**a**) or DLD19 synthetic peptide (**b**) as the substrate. Hydroxylation was monitored based on detection of 4-OH[^{3}H]proline hydroxyproline (**a**) or decarboxylation of 2-oxo-[1-^{14}C]glutarate (**b**).

a

CHX (min)   0 5 10 20 40   0 5 10 20 40

HIF1α

Tubulin

IDH1   R132H
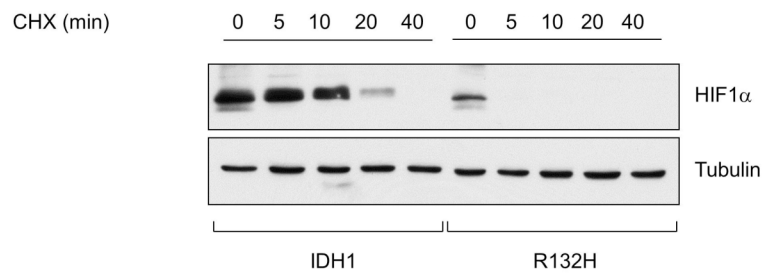
S8. Evidence of enhanced HIF1α hydroxylation and turnover in IDH mutant cells

a, Anti-HIF1α immunoblot analysis of immortalized human astrocytes (passage 12) expressing wild-type or R132H IDH1. Cells were grown under 7.5% oxygen and treated with cycloheximide (50μg/ml) for the indicated amount of time.
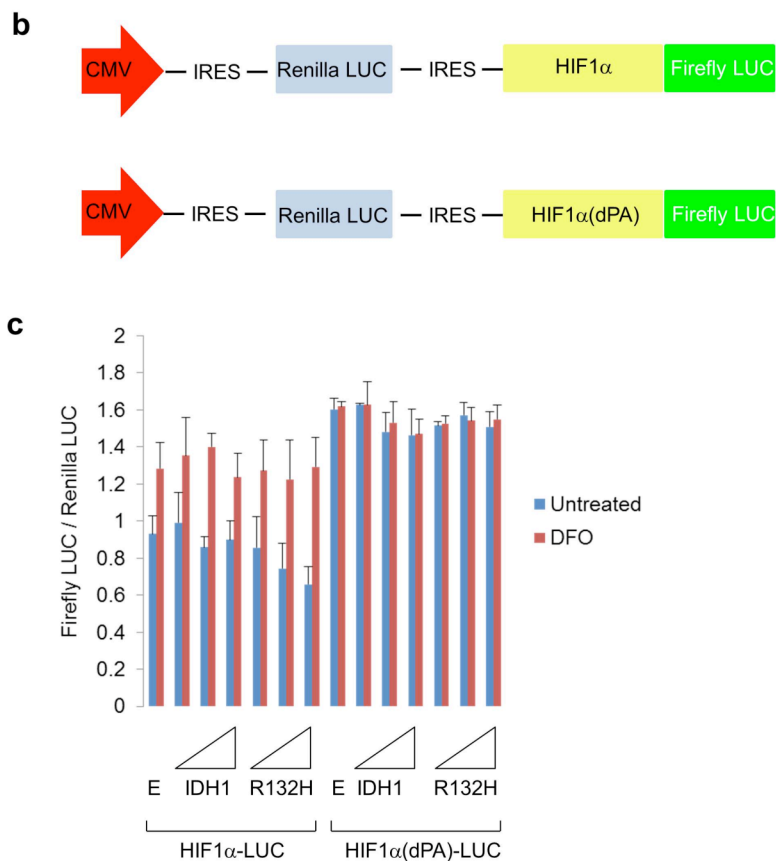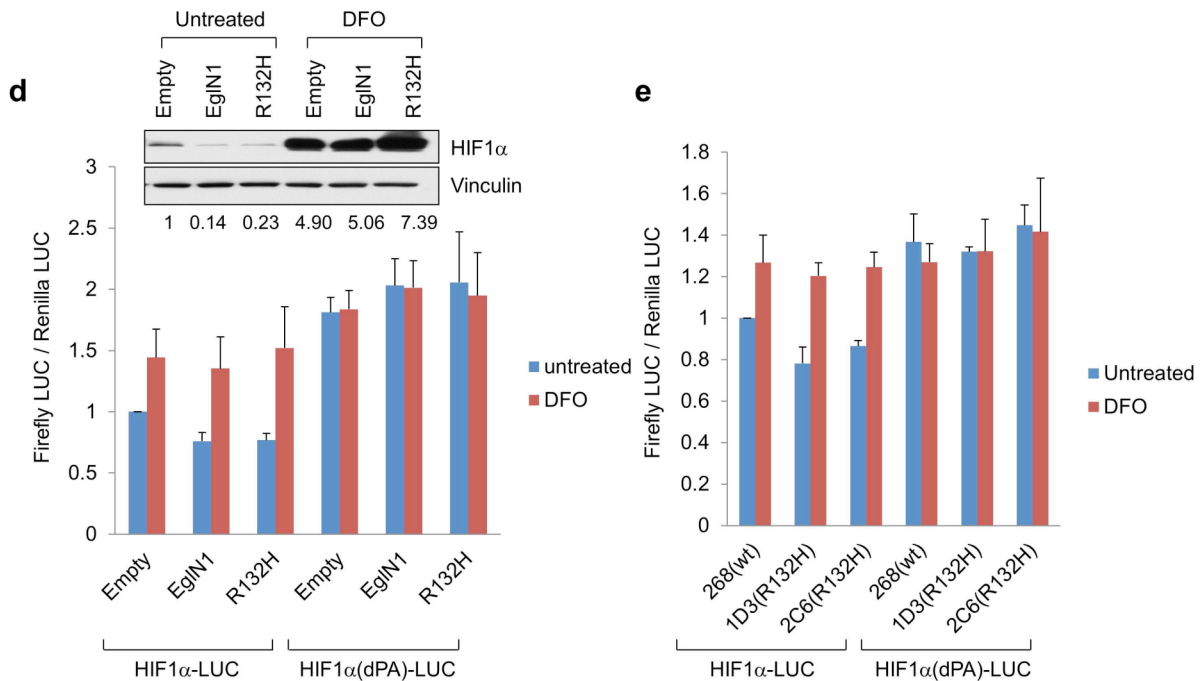
S8. Evidence of enhanced HIF1α hydroxylation and turnover in IDH mutant cells

b, schematic of reporters used to measure HIF1α hydroxylation and turnover. Note that both the HIF1α-firefly luciferase fusion protein and renilla luciferase are encoded by the same transcript. In HIF1α (dPA) both prolyl hydroxylation sites have been converted to alanines.

c, 293T embryonic kidney cells were transfected with the reporter plasmids depicted in (**b**) encoding the wild-type or dPA HIF1α-firefly luciferase fusion proteins. Cells were cotransfected with empty vector or increasing amounts of plasmids encoding wild-type or R132H IDH1, as indicated by the triangles. Where indicated 0.2 mM deferoxamine (DFO) was added to the cells

to inhibit hydroxylase activity. 72 hours after transfection firefly luciferase values were determined and normalized to luciferase.

S8. Evidence of enhanced HIF1α hydroxylation and turnover in IDH1 mutant cells

d and **e,** 293T embryonic kidney cells (**d**) and the indicated HCT116 colorectal cancer cell line subclones (**e**) were transfected with the reporter plasmids depicted in (**b**) encoding the wild-type or dPA HIF1α-firefly luciferase fusion proteins. In (**d**) cells were cotransfected with empty vector or plasmids encoding EglN1 or R132H IDH1. Where indicated 0.2 mM deferoxamine (DFO) was added to the cells to inhibit hydroxylase activity. 72 hours after transfection firefly luciferase values were determined and normalized to luciferase. Inset shows endogenous HIF1α levels. Note that the effect of IDH1 R132H on the HIF1α-luciferase reporter, although modest, was highly reproducible and comparable to the effect of overproducing EglN1. It is possible that fusion to luciferase affects the folding or localization of HIF1α in a manner that alters the

kinetics of its hydroxylation, ubiquitination, and/or proteasomal degradation. Note also that the induction of the HIF1α-luciferase reporter and endogenous HIF1α in 293T cells by DFO was approximately 1.5-fold and 5-fold, respectively. Based on a correction factor of 3.33, the observed 20% decrease in HIF-luciferase reporter activity in these cells by IDH1 R132H would translate into an ~75% decrease in endogenous HIF1α protein level, which approximates the observed result [predicted HIF1α level = 4/(5 x 3.3) = 24% of baseline].
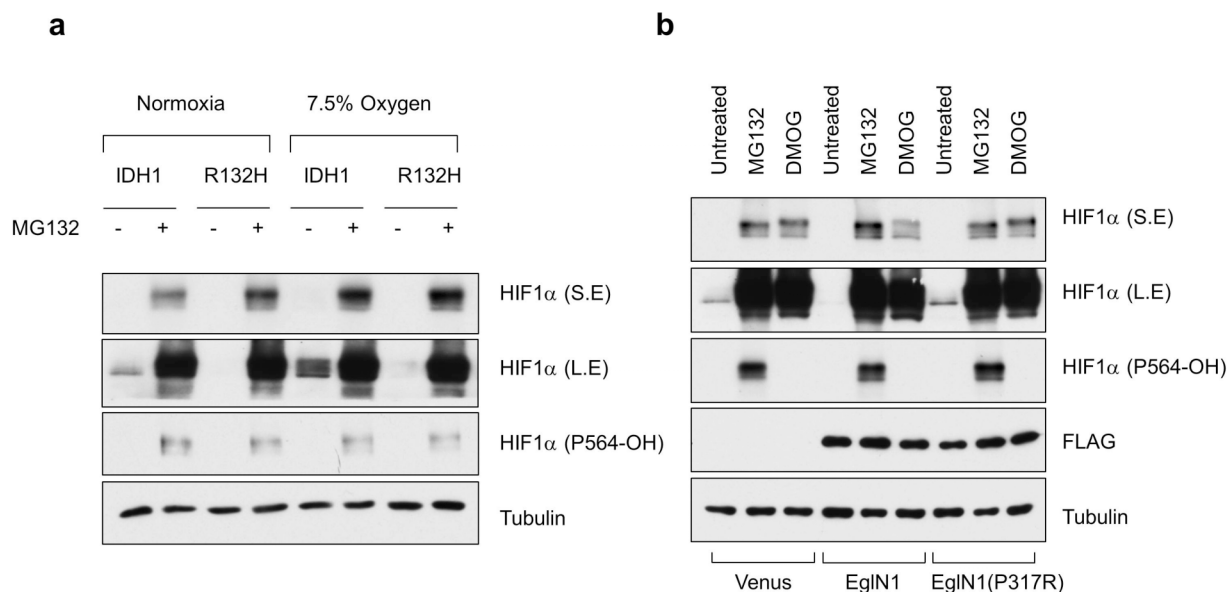
S9. Immunoblot analysis with an antibody specific for hydroxylated HIF1α failed to detect quantitative differences in HIF1α hydroxylation caused by EglN1 overexpression or hypoxia

a,b, Immunoblot analysis of immortalized human astrocytes infected with retroviruses expressing wild-type or R132H IDH1 (passage 10)(**a**) or with lentiviruses encoding Flag-tagged versions of wild-type EglN1, catalytic-dead EglN1(P317R), or venus fluorescent protein (**b**). Cells were grown under 21% (normoxia) or 7.5% oxygen (**a**) and, where indicated, treated with MG132 (25μM) or DMOG (1mM) for 6 hours prior to cell lysis. S.E. and L.E. indicate short and long exposures, respectively, of immunoblots for total HIF1α. HIF1α (P564-OH) indicates

immunoblots with antibody specific for HIF1α hydroxylated on proline 564 (Cell Signaling Technology (Cat #3434) (Comparison of the MG132 and DMOG lanes in (**b**) confirms the specificity of this antibody). In panel (**a**) we failed to detect an increase in HIF1α hydroxylation in R132H using this antibody. HOWEVER, we likewise failed to detect an increase in HIF1α hydroxylation in the positive control cells in which HIF1α turnover was promoted by overexpression of wild-type EglN1 [in (**b**) note decrease in total HIF1α levels in lane 4 compared to lanes 1 and 7 without an increase in HIF1α hydroxylation signal in lane 5 compared with 2 and 8] and failed to detect increased HIF1α hydroxylation in cells grown under 21% oxygen compared to 7.5 % oxygen (**a**). Among several possibilities, MG132 might indirectly affect the rate of HIF1α hydroxylation in addition to blocking HIF1α turnover and therefore confound the interpretation of these experiments. We therefore concluded that alternative strategies were required to determine whether mutant IDH1 affects HIF1α hydroxylation.
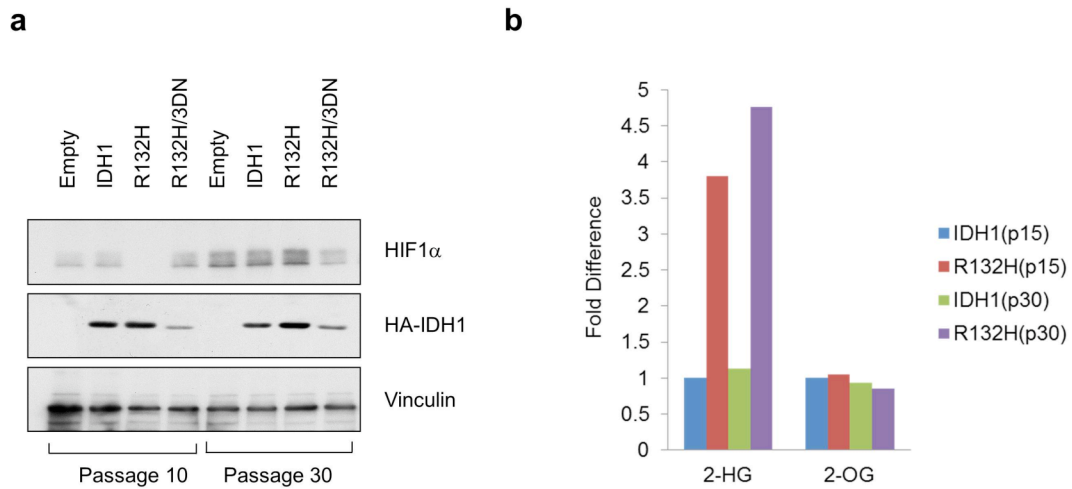
a

b
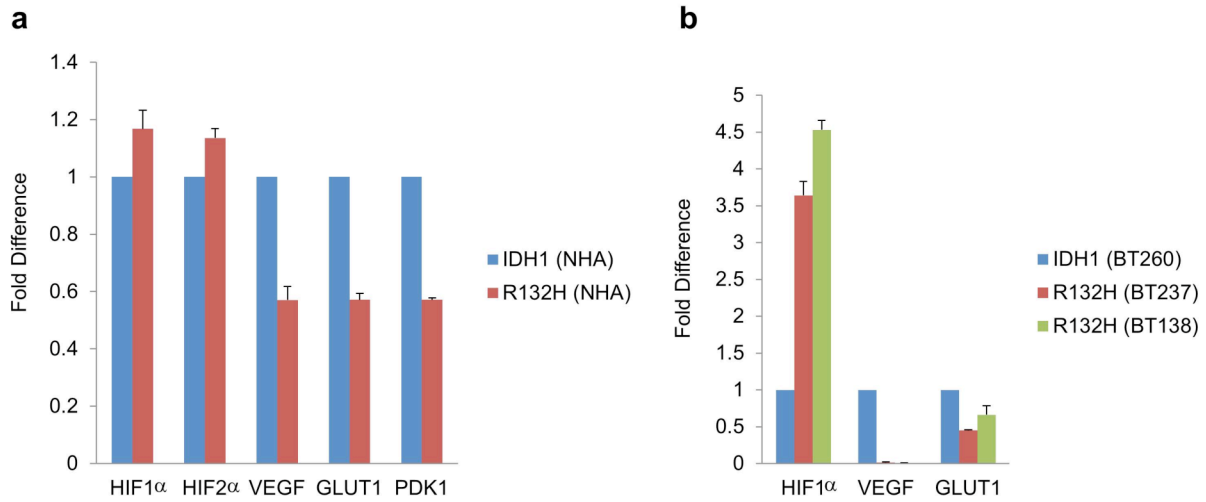
S10. Decreased expression of HIF target genes in IDH1 mutant astrocytes and oligodendroglioma lines.

a,b, Quantitative real-time PCR analysis of cells in Fig 3a (**a**) and Fig 3c (**b**) under normoxic conditions. Error bars = 1 std. dev. (n=3).
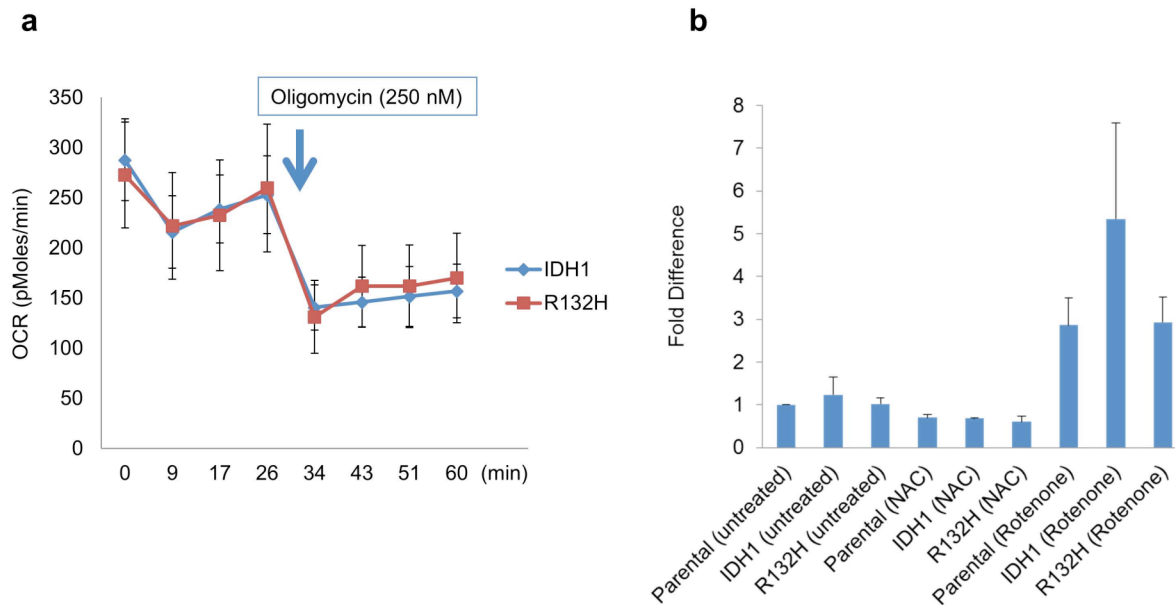
S11. Oxygen consumption and ROS production in IDH1 mutant cell lines

a, b, Measurement of Oxygen Consumption Rate (OCR)(**a**) and Reactive Oxygen Species

(ROS)(**b**) of immortalized human astrocytes (passage 10) expressing the indicated IDH1

variants. OCR was measured using XF24 analyzer (Seahorse Bioscience) 24 hrs after seeding

60,000 cells per well into 24-well microplates. Oligomycin, an inhibitor of ATP synthase, was

added as a control at the indicated time point. (**b**) Cells were incubated for 40 min with 5 μM

CM-H2DCFDA in the presence or absence of 5 mM of NAC (an ROS scavenger) or 20 μM of

Rotenone (an ROS inducer), harvested, resuspended in PBS, and analyzed by FACS.

a

Empty
IDH1
R132H
R132H/3DN
Empty
IDH1
R132H
R132H/3DN

HIF1α

HA-IDH1

Vinculin

Passage 10   Passage 30

b

Fold Difference

■ IDH1(p15)
■ R132H(p15)
■ IDH1(p30)
■ R132H(p30)

2-HG   2-OG

S12. Passage-dependent changes in HIF1α protein levels in immortalized astrocytes expressing IDH1 R132H

a,b, Anti-HA immunoblot (**a**) and LC-MS analysis (**b**) of immortalized human astrocytes infected with retroviruses encoding HA-tagged versions of the indicated IDH1 variants. In (**b**) p15 and p30 indicate passage 15 and 30, respectively.
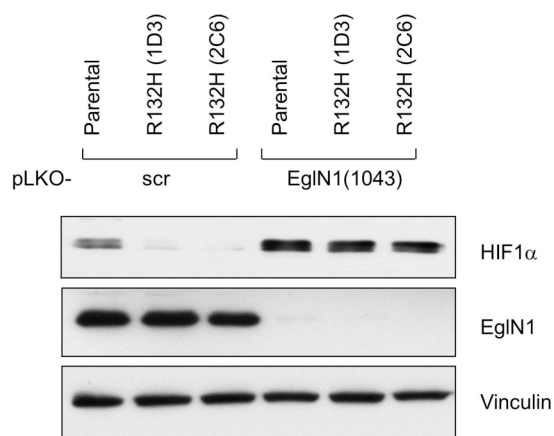
S13. Downregulation of HIF1α by Mutant IDH is EglN-dependent

Anti-HIF1α and EglN1 immunoblot analysis of HCT116 cell lines infected with lentiviruses

encoding the indicated shRNA against EglN1. scr=scrambled shRNA.

| Gene Set	Source
Hypoxia-Benita-Table S6-ProteinInteraction	Hypoxia gene set from Protein Interaction (n=61)
Hypoxia-Benita-Table S6-GSEA	Hypoxia gene set from GSEA (n=99)
HIF1A Gene set assembled by W.G.K.	HIF1A targets suggested by W.G.K. (n=13)
Hypoxia-Benita-Table S6-ProteinDomain	Hypoxia gene set from ProteinDomain (n=15)
Hypoxia-Benita-Table S4	Top200 predicted HIF target genes (n=200)
Hypoxia-Benita-Table S4 - validated	Validated and predicted HIF target genes (n=25)
Hypoxia-Benita-Table S6-TargetScan	Hypoxia gene set from TargetScan (n=28)
Hypoxia-Benita-Table S6-KEGG	Hypoxia gene set from KEGG (n=40)
Hypoxia-Benita-Table S2	Genes with HIF1A binding site in promoter region (n=87)
Hypoxia-Benita-Table S6-Reactome	Hypoxia gene set from Reactome (n=28)
Hypoxia-Benita-Table S6-GSEAOntology	Hypoxia gene set from GSEAOntology (n=74)
Hypoxia-Nickols-Figure 4C	Genes previously identified as direct targets of hypoxia (n=31)
Hypoxia-Benita-Figure 3, U251-Astrocyte	Predicted HIF-target genes responding to hypoxia in U251 and astrocyte cells (n=27)
Hypoxia-Benita-Figure3	Predicted HIF-target genes responding to hypoxia in at least 3 cell types (n=81)

S14. Decreased expression of HIF target genes in *IDH1* mutant brain tumors.

a, Table indicating HIF responsive gene sets used in Supplementary Figures S14b-d to compare the response to HIF activation between *IDH1* mutated and *IDH1* wildtype tumors[3,4]. The gene list constructed by W.G.K. consisted of *CA9, EglN1, EglN3, SLC2A1, BNIP3, ADM, VEGF, PDK1, LOX, PLOD1, CXCR4, P4HA1, and ANKRD37*.
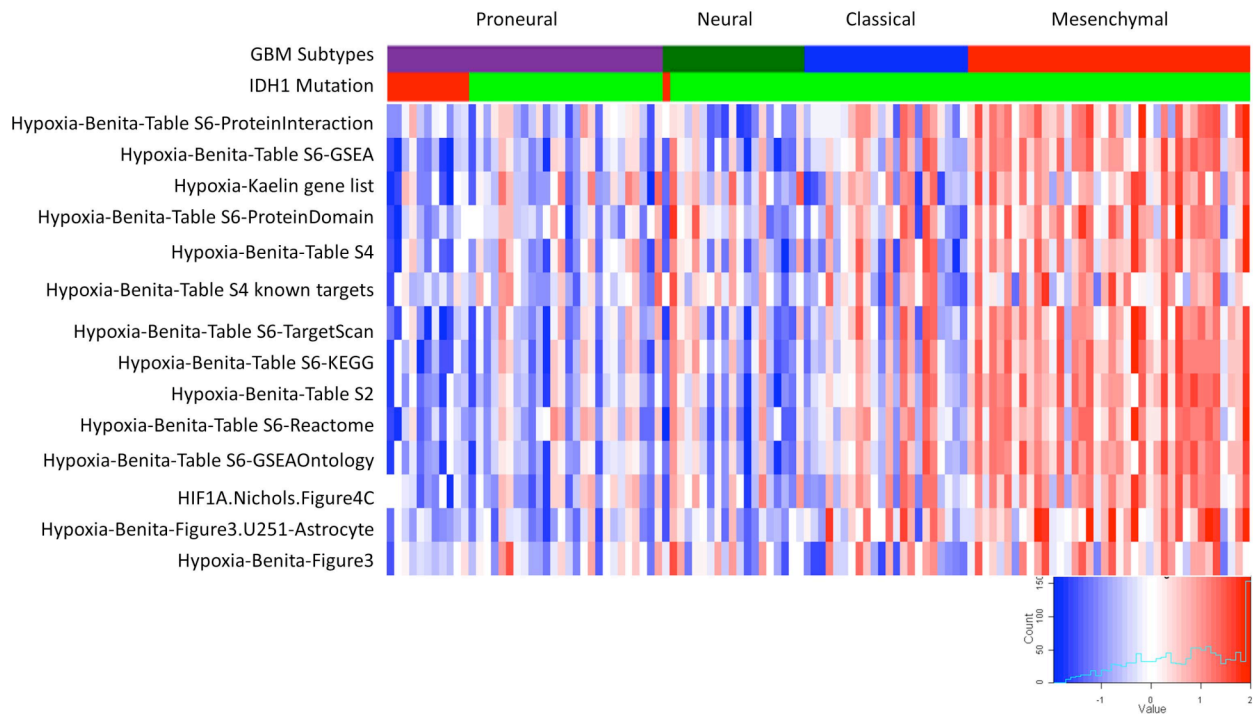
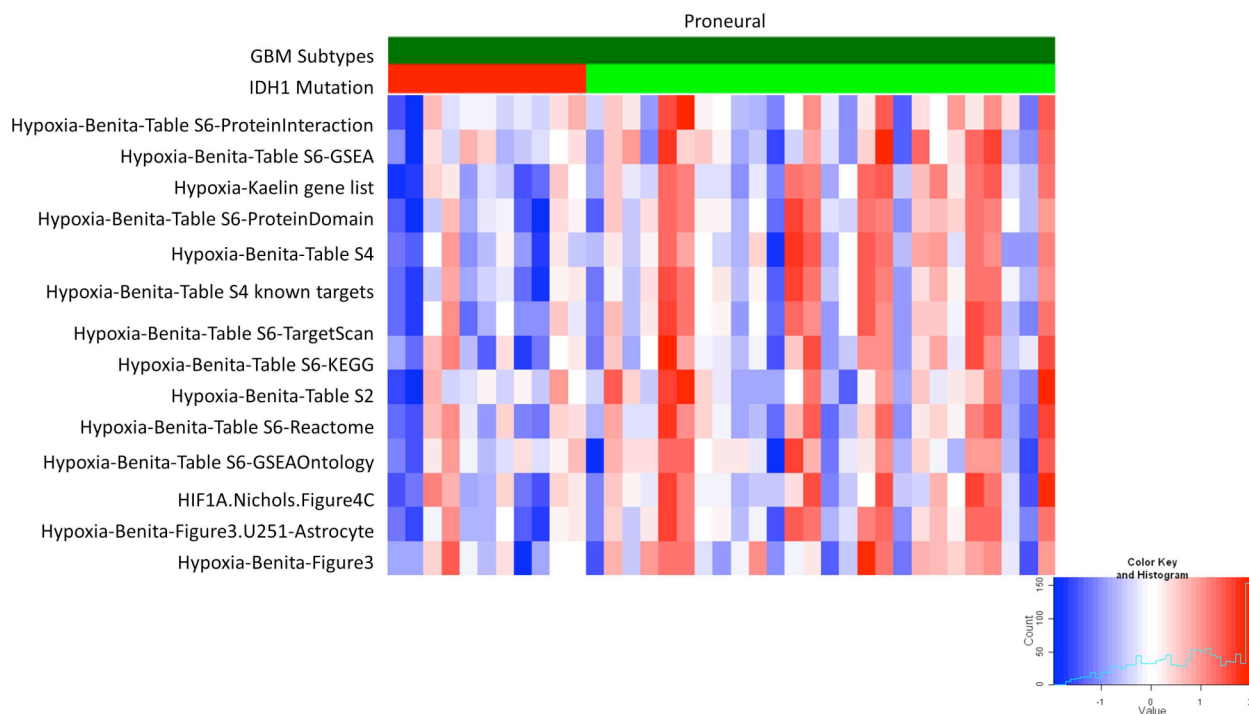**S14. Decreased expression of HIF target genes in *IDH1* mutant brain tumors.**

b, Analysis of 116 expression profiles from brain tumor samples from The Cancer Genome Atlas [5-7] for which IDH1 mutation status was available using thirteen gene sets representing response to HIF activation. Gene sets used are described in Supplementary Figure S14a. The activation status of each gene set in each samples was measured using single sample Gene Set Enrichment Analysis[8]. Blue indicates lack of activation of a gene set in a given sample, red indicates activation of a gene set. Tumors were clustered based on gene expression-defined brain tumor subtypes as described[6]. *IDH1* status is indicated (red = mutant and green = wild-type).
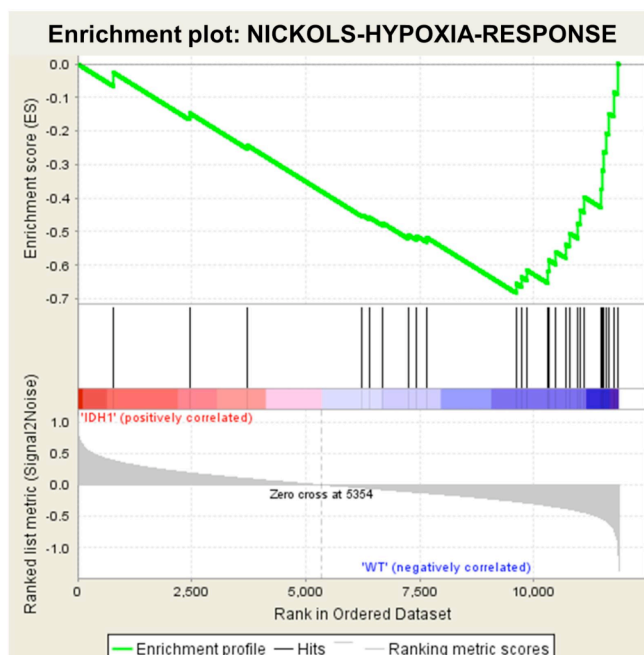
S14. Decreased expression of HIF target genes in *IDH1* mutant Proneural brain tumors.

c, Gene set enrichment analysis using the data depicted in Fig 3f, comparing the expression of

the Nickols HIF target gene set[4] between eleven tumor samples with *IDH1* mutation and twenty

six tumor samples with *IDH1* wildtype. All samples clustered in the Proneural expression

subtype. In short, all genes in the expression profiles were ranked by the difference in expression

between the *IDH1* mutant/*IDH1* wildtype tumors. The vertical black bars represent the position

of each of the 27 genes in the HIF gene set in the ranked gene list, with genes upregulated in

IDH1 wild-type tumors relative to *IDH1* mutant tumors appearing toward the left and genes

upregulated in *IDH1* mutant tumors relative to *IDH1* wild-type tumors toward the right. The

graph in green shows the corresponding enrichment score and indicates that the Nickols HIF

target gene set is activated at a significantly lower level in *IDH1* mutant tumors compared to

IDH1 wild-type tumors. The graph in grey at the bottom shows the signal to noise score for each

gene in the ranked list.

**S14. Decreased expression of HIF target genes in *IDH1* mutant brain tumors.**

d, Analysis of thirty seven expression profiles from brain tumor samples from The Cancer Genome Atlas[5-7] from the Proneural gene expression subtype for which *IDH1* mutation status was available, using thirteen gene sets representing response to HIF activation. Gene sets used are described in Supplementary Figure S14a. The activation status of each gene set in each samples was measured using single sample Gene Set Enrichment Analysis[8]. Blue indicates lack of activation of a gene set in a given sample, red indicates activation of a gene set. Tumors were clustered based on gene expression-defined brain tumor subtypes as described[6]. *IDH1* status is indicated (red = mutant and green = wild-type).

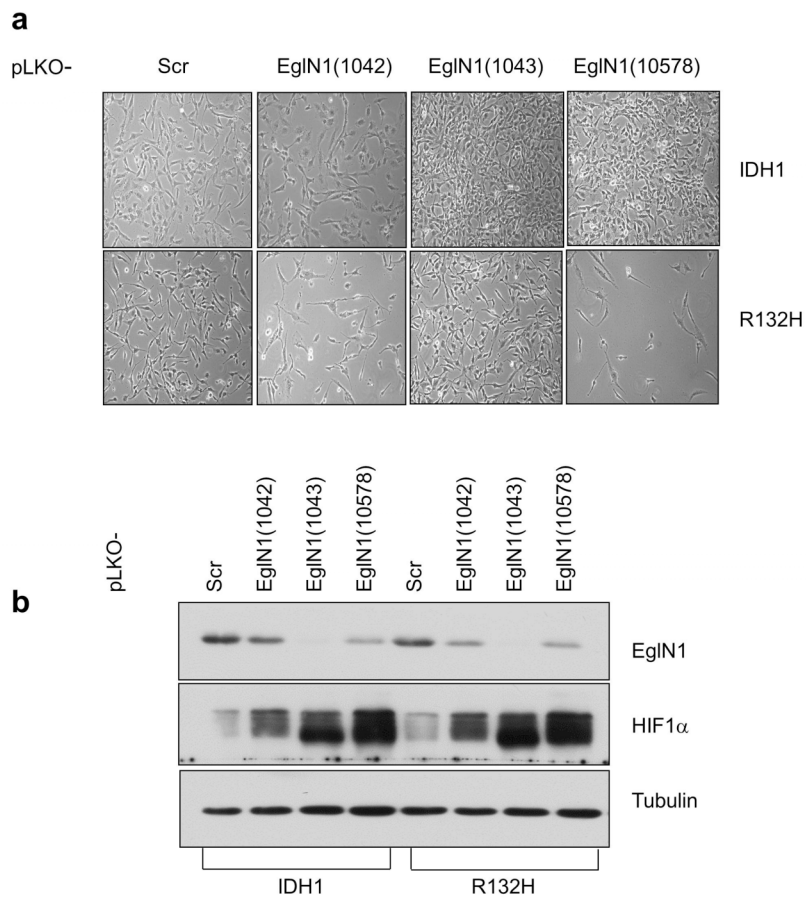## S15. shRNA-mediated downregulation of HIF1α protein

Immunoblot analysis of immortalized human astrocytes (passage 15) after stable infection with

lentiviruses encoding the indicated shRNAs against HIF1α. Scr= scrambled shRNA.

Lentiviruses were obtained from the TRC collection of the Broad Institute, Cambridge, MA.
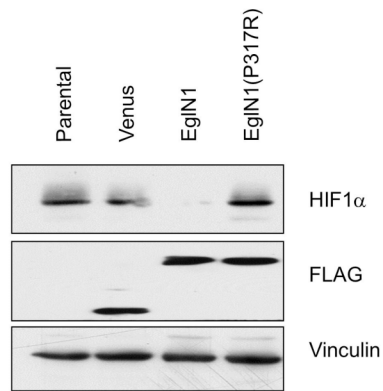
S16. Production of exogenous EglN1 and EglN1 (P317R)

Immunoblot analysis of immortalized human astrocytes (passage 15) after stable infection with lentiviruses encoding Flag epitope-tagged versions of EglN1, EglN1 (P317R), or venus fluorescent protein.

a

pLKO- | Scr | EglN1(1042) | EglN1(1043) | EglN1(10578)

IDH1

R132H

b

pLKO- | Scr | EglN1(1042) | EglN1(1043) | EglN1(10578) | Scr | EglN1(1042) | EglN1(1043) | EglN1(10578)

EglN1

HIF1α

Tubulin

IDH1   R132H

S17. Antiproliferative effects of EglN1 shRNAs in IDH1 R132H cells

a,b. Photomicrographs (**a**) and immunoblot analysis (**b**) of immortalized human astrocytes (passage 25) expressing wild-type (IDH1) or mutant (R132H) IDH1 after infection with lentiviruses encoding the indicated shRNAs against EglN1. Scr = scrambled shRNA. Lentiviruses were obtained from the TRC collection of the Broad Institute, Cambridge.

c

d
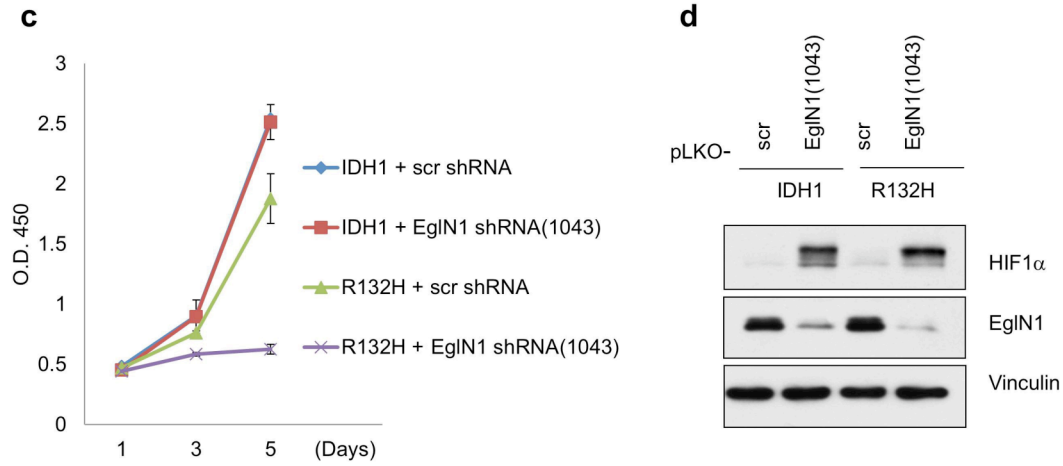
S17. Antiproliferative effects of EglN1 shRNAs in IDH1 R132H cells

c,d Proliferation (**c**) and immunoblot analysis (**d**) of human astrocytes (passage 25) expressing wild-type or R132H IDH1 and an shRNA against EglN1 (or scrambled control).
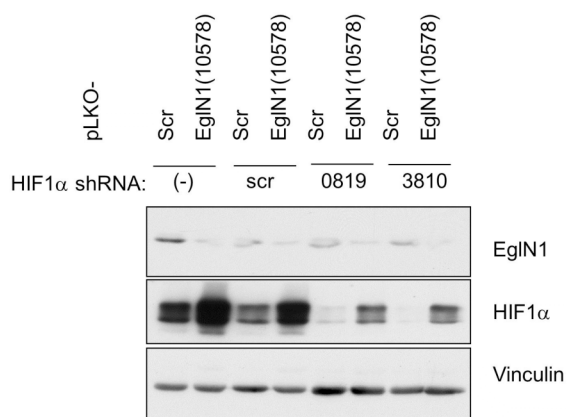
**S18. shRNA-mediated downregulation of HIF1α and EglN1.**

Immunoblot analysis of immortalized human astrocytes (passage 15) expressing IDH1 R132H after sequential infections with lentiviruses encoding the indicated shRNAs against EglN1 and HIF1α. Scr = scrambled shRNA. Cells were infected with HIF1α (or scr) lentiviruses 2 weeks before infection with the EglN1 (or scr) lentivirus. Lentiviruses were obtained from the TRC collection of the Broad Institute, Cambridge, MA.
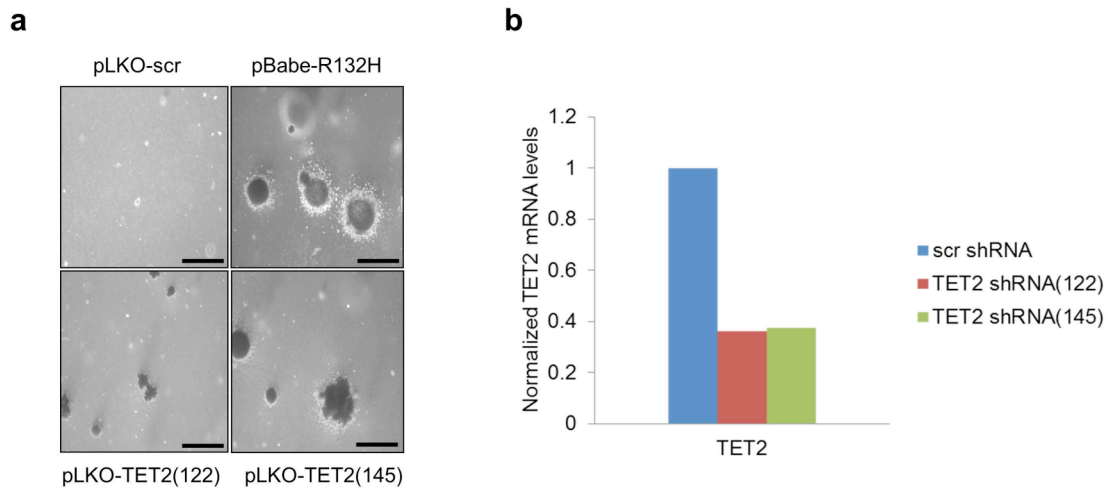
S19. Enhanced soft agar growth of human astrocytes after downregulation of TET2

a and **b.** Soft agar growth (**a**) and quantitative real-time PCR analysis (**b**) of immortalized human astrocytes (passage 12) infected with lentiviruses encoding the indicated TET2 shRNAs. Cells infected with a retrovirus encoding IDH1 R132H or a lentivirus encoding a scrambled (scr) shRNA served as positive and negative controls, respectively. In (**a**) cells were assayed after ~ 15 passage. In (**b**) cells were assayed 2 weeks after viral infection. TET2 mRNA levels were first normalized to beta actin mRNA levels and then expressed relative to normalized TET2 levels in cells expressing scr shRNA. Bars in (**a**) = 0.5 mm.
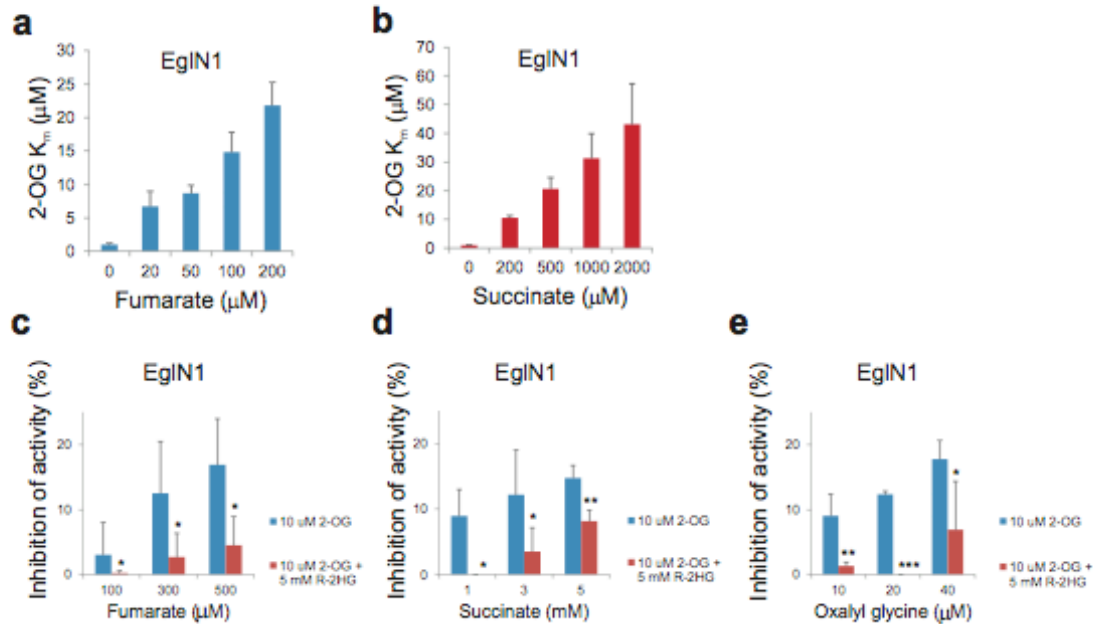
S20. R-2HG antagonizes 2-OG-competitive EglN inhibitors

a,b, Apparent 2-OG K_m values for recombinant EglN1 (1-426) in the presence of increasing amounts of fumarate and succinate. K_m values were determined as described previously [9] based on stoichiometric release of $^{14}CO_2$ from 2-oxo-[1-^{14}C]glutarate during hydroxylation of a synthetic HIF1α peptide (DLD19). The data are average +/- SD of three independent assays done in duplicate. **c-e,** Combination of 2-OG and R-2HG is more resistant to inhibition of EglN1 activity by 2-OG-competitive antagonists than is 2-OG alone. EglN1 activity was determined based on generation of 4-OH[^{3}H]proline using L-[2,3,4,5-^{3}H]proline-labeled HIF-1α ODDD as substrate. The data are average +/- SD of 3-5 independent assays done in duplicate. * $P<0.05$, **$P<0.005$, ***$P<0.001$ compared to 10 uM 2-OG alone.

1   Dang, L. et al. Cancer-associated IDH1 mutations produce 2-hydroxyglutarate. Nature 462, 739-744 (2009).

2   Chowdhury, R. et al. The oncometabolite 2-hydroxyglutarate inhibits histone lysine demethylases. EMBO Rep, 12, 463-469 (2011).

3   Benita, Y. et al. An integrative genomics approach identifies Hypoxia Inducible Factor-1 (HIF-1)-target genes that form the core response to hypoxia. Nucleic Acids Res 37, 4587-4602, (2009).

4   Nickols, N. G., Jacobs, C. S., Farkas, M. E. & Dervan, P. B. Modulating hypoxia-inducible transcription by disrupting the HIF-1-DNA interface. ACS Chem Biol 2, 561-571, (2007).

5   Comprehensive genomic characterization defines human glioblastoma genes and core pathways. Nature 455, 1061-1068 (2008).

6   Verhaak, R. G. et al. Integrated genomic analysis identifies clinically relevant subtypes of glioblastoma characterized by abnormalities in PDGFRA, IDH1, EGFR, and NF1. Cancer Cell 17, 98-110 (2010).

7   Wang, X. V., Verhaak, R. G., Purdom, E., Spellman, P. T. & Speed, T. P. Unifying gene expression measures from multiple platforms using factor analysis. PLoS One 6, e17691 (2011).

8   Subramanian, A. et al. Gene set enrichment analysis: a knowledge-based approach for interpreting genome-wide expression profiles. Proc Natl Acad Sci U S A 102, 15545-15550 (2005).

9   Koivunen, P. et al. Inhibition of hypoxia-inducible factor (HIF) hydroxylases by citric acid cycle intermediates: possible links between cell metabolism and stabilization of HIF. J Biol Chem 282, 4524-4532 (2007).